molecular pharmaceutics

articles

Chemical Substituent Effect on Pyridine Permeability and Mechanistic Insight from Computational Molecular Descriptors

I-Jen Chen, Rajneesh Taneja, Daxu Yin, Paul R. Seo, David Young, Alexander D. MacKerell, Jr.,* and James E. Polli*

Department of Pharmaceutical Sciences, School of Pharmacy, University of Maryland, Baltimore, Maryland 21201

Received November 3, 2005

Abstract: The objective was (1) to evaluate the chemical substituent effect on Caco-2 permeability, using a congeneric series of pyridines, and (2) compare molecular descriptors from a computational chemistry approach against molecular descriptors from the Hansch approach for their abilities to explain the chemical substituent effect on pyridine permeability. The passive permeability of parent pyridine and 14 monosubstituted pyridines were measured across Caco-2 monolayers. Computational chemistry analysis was used to obtain the following molecular descriptions: solvation free energies, solvent accessible surface area, polar surface area, and cavitation energy. Results indicate that the parent pyridine was highly permeable and that chemical substitution was able to reduce pyridine permeability almost 20-fold. The substituent effect on permeability provided the following rank order: 3-COO^- < 4-NH_2 < 3-$CONH_2$ < 3-Cl < 3-CHO < 3-OH < 3-CH_2OH < 3-C_6H_5 < 3-NH_2 < 3-$CH_2C_6H_5$ < 3-C_2H_5 < **3-H** < 3-CH_3 < 3-F < 4-C_6H_5. This substituent effect was better explained via molecule descriptors from the computational chemistry approach than explained by classic descriptors from Hansch. Computational descriptors indicate that aqueous desolvation, but not membrane partitioning per se, dictated substituent effect on permeability.

Keywords: Chemical substituent; permeability; computational chemistry; Caco-2; QSAR; aqueous desolvation

Introduction

Modern drug discovery methods require the rational design of favorable oral absorption and bioavailability during compound development. In silico approaches of screening for oral absorption and/or intestinal permeability offer great potential to achieve this goal.[1−4] Such computer-based methods have increasing utilization because of their ability to predict absorption/permeability of diverse compounds from compound structure.[5−16] Interestingly, and in contrast to traditional quantitative-structure activity relationship (QSAR)

* To whom correspondence should be addressed: Department of Pharmaceutical Sciences, School of Pharmacy, University of Maryland, Baltimore, MD, 21201. Tel: (410) 706−8292. Fax: (410) 706−5017. E-mail: jpolli@rx.umaryland.edu; amackere@rx.umaryland.edu.

(1) Stenberg, P.; Luthman, K.; Artursson P. Virtual screening of intestinal drug permeability. *J. Controlled Release* **2000**, *65*, 231−243.

(2) van de Waterbeemd, H. Which in vitro screens guide the prediction of oral absorption and volume of distribution? *Basic Clin. Pharmacol. Toxicol.* **2005**, *96*, 162−6.

(3) Clark, D. E.; Grootenhuis, P. D. Predicting passive transport in silico—history, hype, hope. *Curr. Top. Med. Chem.* **2003**, *3*, 1193−1203.

(4) Egan, W. J.; Lauri, G. Prediction of intestinal permeability. *Adv. Drug Delivery Rev.* **2002**, *54*, 273−289.

(5) Winiwarter, S.; Bonham, N. M.; Ax, F.; Hallberg, A.; Lennernas, H.; Karlen, A. Correlation of human jejunal permeability (in vivo) of drugs with experimentally and theoretically derived parameters. A multivariate data analysis approach. *J. Med. Chem.* **1998**, *41*, 4939−4949.

10.1021/mp050096+ CCC: $33.50 © 2006 American Chemical Society
Published on Web 09/29/2006

methods in drug design, there is limited data that measures the influence of chemical substituents on drug intestinal permeability. Anderson and colleagues observed functional groups that had the following rank-order effect on the intrinsic permeability of substituted *p*-toluic acids and *p*-methylhippuric acids across artificial lipid bilayers: $-CONH_2 < -COOH < -OH < -CH_2OH < -Cl < -H$.[17] Given the general lack of information concerning chemical group effects on permeability, one objective of the present study was to evaluate the chemical substituent effect on Caco-2 permeability using a congeneric series of pyridines. Caco-2 monolayers were selected as a permeability model because (a) biological bilayers may be expected to be exhibit a sensitivity to chemical substituents that differs from the sensitivity of an artificial bilayer[18] and (b) Caco-2 monolayers are used widely to assess lead compound permeability and predict oral absorption.[19] A congeneric series of pyridine was selected because pyridine is a common scaffold in real drug structures.[20]

A second objective was to compare the relative abilities of molecular descriptors from a computational chemistry approach versus those from the Hansch approach, to explain the chemical substituent effect on pyridine permeability. Classical Hansch parameters π, σ, and E_s have been employed widely to describe substituent effects on drug activity[21] and would appear to serve as a reference for evaluating a computational chemistry approach to explain functional group effects. The computational approach taken here included solute−solvent interactions (e.g., solute−water interactions) because aqueous desolvation of the solute is a potentially rate-limiting step in membrane permeation.[22] To date, the majority of computational methods that describe permeability in terms of molecular descriptors only consider the solute, and not explicit solute−solvent interactions. To compare the computational chemistry approach and the Hansch approach, we have measured the permeabilities of a series of substituted pyridines through Caco-2 cells as well as obtained computational and Hansch-based molecular descriptors for the respective compounds. Regression analysis between the experimental data and both types of descriptors was then performed to evaluate the two approaches. A model for the molecular events dictating the permeability of substituted pyridines was obtained and highlights the computational chemistry approach to better explain pyridine permeability.

Experimental Section

Materials. Fifteen pyridines were purchased from Aldrich Chemical Co. (Milwaukee, MI). ^{14}C-Mannitol was purchased from New England Nuclear (Boston, MA). Dulbecco's Modified Eagles Media (DMEM) and Hank's Balanced Salt Solution (HBSS) were obtained from Sigma Chemical Co. (St. Louis, MO). Nonessential amino acids (NEAA), fetal bovine serum (FBS), trypsin, penicillin-streptomycin, and HEPES buffer were purchased from Biofluids Inc. (Rockville, MD). Caco-2 cell line (passage number 17) was obtained from American Type Culture Collection (Rockville, MD).

Cell Culture and Caco-2 Permeability Measurement. Caco-2 cells were grown in T-150 flasks at 37 °C in an

(6) Stenberg, P.; Norinder, U.; Luthman, K.; Artursson, P. Experimental and computational screening models for the prediction of intestinal drug absorption. *J. Med. Chem.* **2001**, *44*, 1927−1937.
(7) Krarup, L. H.; Christensen, I. T.; Hovgaard, L.; Frokjaer, S. Predicting drug absorption from molecular surface properties based on molecular dynamics simulations. *Pharm. Res.* **1998**, *15*, 972−978.
(8) Norinder, U.; Osterberg, T.; Artursson, P. Theoretical calculation and prediction of intestinal absorption of drugs in humans using MolSurf parametrization and PLS statistics. *Eur. J. Pharm. Sci.* **1999**, *8*, 49−56.
(9) Wessel, M. D.; Jurs, P. C.; Tolan, J. W.; Muskal, S. M. Prediction of human intestinal absorption of drug compounds from molecular structure. *J. Chem. Inf. Comput. Sci.* **1998**, *38*, 726−735.
(10) Veber, D. F.; Johnson, S. R.; Cheng, H. Y.; Smith, B. R.; Ward, K. W.; Kopple, K. D. Molecular properties that influence the oral bioavailability of drug candidates. *J. Med. Chem.* **2002**, *45*, 2615−2623.
(11) Zhao, Y. H.; Abraham, M. H.; Le, J.; Hersey, A.; Luscombe, C. N.; Beck, G.; Sherborne, B.; Cooper, I. Rate-limited steps of human oral absorption and QSAR studies. *Pharm. Res.* **2002**, *19*, 1446−1457.
(12) Yamashita, F.; Wanchana, S.; Hashida, M. Quantitative structure/property relationship analysis of Caco-2 permeability using a genetic algorithm-based partial least-squares method. *J. Pharm. Sci.* **2002**, *91*, 2230−2239.
(13) Andrews, C. W.; Bennett, L.; Yu, L. X. Predicting human oral bioavailability of a compound: development of a novel quantitative structure-bioavailability relationship. *Pharm. Res.* **2000**, *17*, 639−644.
(14) Ekins, S.; Durst, G. L.; Stratford, R. E.; Thorner, D. A.; Lewis, R.; Loncharich, R. J.; Wikel, J. H. Three-dimensional quantitative structure-permeability relationship analysis for a series of inhibitors of rhinovirus replication. *J. Chem. Inf. Comput. Sci.* **2001**, *41*, 1578−1586.
(15) Kulkarni, A.; Han, Y.; Hopfinger, A. J. Predicting Caco-2 cell permeation coefficients of organic molecules using membrane-interaction QSAR analysis. *J. Chem. Inf. Comput. Sci.* **2002**, *42*, 331−342.
(16) Ginoz, S.; Rey, S.; Boss, G.; Bunge, A. L.; Guy, R. H.; Carrupt, P. A.; Reist, M.; Testa, B. Quantitative structure-permeation relationships for solute transport across silicone membranes. *Pharm. Res.* **2002**, *19*, 1622−1629.
(17) Mayer, P. T.; Xiang, T. X.; Anderson, B. D. Independence of substituent contributions to the transport of small molecule permeants in lipid bilayers. *AAPS PharmSci.* **2000**, *2*, E14.
(18) Xiang, T.; Anderson, B. D. Influence of a transmembrane protein on the permeability of small molecules across lipid membranes. *J. Membr. Biol.* **2000**, *173*, 187−201.
(19) Lentz, K. A.; Hayashi, J.; Lucisano, L. J.; Polli, J. E. Development of a more rapid, reduced serum culture system for Caco-2 monolayers and application to biopharmaceutics classification system. *Int. J. Pharm.* **2000**, *200*, 41−51.
(20) Bemis, G. W.; Murcko, M. A. The properties of known drugs. 1. Molecular frameworks. *J. Med. Chem.* **1996**, *39*, 2887−2893.
(21) Hansch, C.; Leo, A. *Exploring QSAR*; American Chemical Society: Washington, DC, 1995.
(22) Burton, P. S.; Conradi, R. A.; Ho, N. F.; Hilgers, A. R.; Borchardt, R. T. How structural features influence the biomembrane permeability of peptides. *J. Pharm. Sci.* **1996**, *85*, 1336−1340.

atmosphere of 5% CO_2 and 95% relative humidity, as described previously.[23] Growth medium consisted of DMEM, 10% FBS, 1% penicillin-streptomycin, and DEAA and was adjusted to pH 7.2 with 0.1 N NaOH. Cells (between passage number 35 and 48) were trypsinized using 0.25% trypsin and 0.2% EDTA solution. The cells were seeded on Costar Transwell inserts (0.4 mm, 4.71 cm^2) at a seeding density of 1×10^5 cells/cm^2 and were cultured for 21−25 days prior to utilization in conducting transport studies.

Monolayers with TEER values of at least 850 Ωcm^2 in the culture media at room temperature were used for permeability studies. Transport studies were conducted in HBSS at pH 6.8. For apical-to-basolateral (A−B) studies, a 1 mM substituted pyridine solution (1.5 mL) was placed in the apical chamber and 2.5 mL of HBSS was added to the basolateral chamber. At predetermined time intervals, the filter was carefully moved to a new basolateral chamber in order to sample flux over time. Aliquots were withdrawn from the basolateral chamber and analyzed to determine the pyridine mass that permeated across the Caco-2 cell monolayer. Basolateral-to-apical (B−A) studies were performed in a similar manner; samples were withdrawn from apical chamber at selected time intervals and replaced with an equal amount of HBSS. At the end of each experiment, the monolayer integrity was assessed via a ^{14}C-mannitol permeability study. The mannitol permeability was less than 1×10^{-6} cm/s, indicating acceptable monolayer integrity. As monolayers were used from four passages, the permeability of pyridine was assessed on each of the four occasions; pyridine permeability did not vary with occasion (ANOVA $p = 0.9$). Permeability was calculated from

$$P_{\text{eff}} = \frac{dC_R}{dt}\frac{V_R}{AC_0} \quad (1)$$

where V_R is the volume of the receiver compartment, A is the membrane surface area, and C_0 is the donor concentration. Mass balance analysis was conducted to determine the percent of initial mass that could be accounted for at the conclusion of the study. For each pyridine, the mass balance ranged from 80% to 105%, which was deemed acceptable. Permeability is reported as mean ±SEM.

Computational Chemistry Methods. A computational chemistry approach was applied to derive several molecular descriptors. Calculations were performed using the semiempirical quantum chemical program AMSOL 5.4.[24] Along with parent pyridine, each molecule consisted of a pyridine ring with a substituent at the 3′ or 4′ position (Figure 1). Because Caco-2 permeability studies were performed at pH 6.8, the ionization state of each compound was assigned based on its experimental pK_a value. For the few pyridines with no experimentally reported pK_a values, their computationally estimated pK_a values were used.[25]

R = H, CH_3, C_2H_5, CH_2OH, C_6H_5, $CH_2C_6H_5$, CHO, COO^-, $CONH_2$, F, Cl, OH, NH_2
R' = C_6H_5, NH_2

Figure 1. Pyridine analogues.

Geometries of the 15 compounds were fully optimized using the semiempirical Austin Model 1 (AM1)[26] Hamiltonian in the gas phase at the appropriate ionic state. For congeners whose substituents have rotational freedom, the potential energy surfaces of the associated dihedral angle were determined and the conformer of the lowest energy was selected. Free energies of solvation in water and hexane were calculated with the AM1-SM2[27] and AM1-SM4[28] models, respectively. For calculations in the solvents, the previously optimized geometry from the gas phase was adopted. Reoptimization of the structure in the presence of the solvent had only a minor impact on the geometry and energetics, compared to the considerable computational cost (results not shown).

Four types of physicochemical properties were calculated. First, the solvation free energies in water (ΔG_w) and hexane (ΔG_h) were obtained as the difference between the total free energies in water or hexane, respectively, and the gas phase heat of formation. Second, the solvent accessible surface area (SASA) of each compound was calculated in the presence of water or hexane using the method of Lee and Richards, where a sphere representing the solvent molecule was used to probe along the van der Waals surface.[29,30] Third, the polar surface area (*PSA*) was defined as the sum of solvent accessible surface area of all chlorine, fluorine, nitrogen, and oxygen atoms and hydrogens covalently attached to these heteroatoms,[31] as determined in the AM1-SM2 and AM1-SM4 calculations. *SASA*s and *PSA*s were calculated using

(23) Polli, J. E.; Ginski, M. J. Human drug absorption kinetics and comparison to Caco-2 monolayer permeabilities. *Pharm. Res.* **1998**, *15*, 47−52.

(24) Cramer, C. J.; Lynch, G. C.; Hawkins, G. D.; Giesen, D. J.; Truhlar, D. G.; Liotard, D. A. AMSOL 5.4. *QCPE Bull.* **1994**, *14*, 55−70.

(25) Chen, I.-J.; MacKerell, A. D., Jr. Computation of the influence of chemical substitution on the pK_a of pyridine using semiempirical and ab initio methods. *Theor. Chem. Acc.* **2000**, *103*, 483−494.

(26) Dewar, M. J. S.; Zoebisch, E. G.; Healy, E. F.; Stewart, J. J. P. AM1: a new general purpose quantum mechanical molecular mode. *J. Am. Chem. Soc.* **1985**, *107*, 3902−3909.

(27) Cramer, C. J.; Truhlar, D. G. AM2-SM2 and PM3-SM3 parametrized SCF solvation models for free energies in aqueous solution. *J. Comput-Aided Mol. Des.* **1992**, *6*, 629−666.

(28) Giesen, D. J.; Storer, J. W.; Cramer, C. J.; Truhlar, D. G. General semiempirical quantum mechanical solvation for nonpolar solvation free energies. *n*-hexadecane. *J. Am. Chem. Soc.* **1995**, *117*, 1057−1068.

(29) Lee, B.; Richards, F. M. The interpretation of protein structures: estimation of static accessibility. *J. Mol. Biol.* **1971**, *55*, 379−400.

(30) Richards, F. M. Areas, volumes, packing and protein structure. *Annu. Rev. Biophys. Bioeng.* **1977**, *6*, 151−176.

Table 1. Hansch Properties Values

substituent	π	π_+	π_-	σ	E_s
3-COO^-	−4.36	0	−4.36	−0.10	−0.55
4-NH_2	−1.19	0	−1.19	−0.66	−0.61
3-$CONH_2$	−1.49	0	−1.49	0.28	−0.55
3-Cl	0.53	0.53	0	0.37	−0.97
3-CHO	−0.65	0	−0.65	0.35	−0.55
3-OH	−0.67	0	−0.67	0.12	−0.55
3-CH_2OH	−0.62	0	−0.62	0.00	−1.21
3-C_6H_5	1.96	1.96	0	0.06	−3.43
3-NH_2	−1.19	0	−1.19	−0.16	−0.61
3-$CH_2C_6H_5$	2.01	2.01	0	−0.08	−1.51
3-C_2H_5	1.02	1.02	0	−0.07	−1.31
3-H	0.00	0.00	0	0.00	0.00
3-CH_3	0.50	0.50	0	−0.07	−1.24
3-F	−0.17	0	−0.17	0.34	−0.55
4-C_6H_5	1.96	1.96	0	−0.01	−3.43

the conformation at the global energy minimum for each tested compound. Because the substituents in this pyridine series were relatively rigid and small, variation in *SASA* or *PSA* due to substituent flexibility was assumed to be negligible. Fourth, the free energy for creating a cavity in the solvent to accommodate a solute, and for the changes in dispersion interactions and solvent structure that accompany the solvation process, were evaluated for each compound.[28] This parameter was denoted cavitation energy or *CDS* and was computed for both water and hexane as solvent. Additionally, the number of hydrogen bonds (*HB*) was counted as the number of lone electron pairs (i.e., number of hydrogen bond acceptors) and hydrogens attached to an N or O (i.e., hydrogen bond donors). *HB* was counted via an in-house script.

Simple Linear Regression Analysis of Computational Chemistry Parameters. As an intermediate step in deriving a final model that employed multiple linear regression to relate permeability to computational chemistry parameters, simple (i.e., single) linear regression was performed between permeability and each individual computational chemistry molecular descriptor [i.e., ΔG_w, $SASA_w$, PSA_w, fPSA_w, CDS_w, *HB*, ΔG_h, $SASA_h$, PSA_h, fPSA_h, CDS_h, and molecular weight (M_w)]. This analysis was conducted in order to elucidate the general influence of each parameter on permeability. Regression was performed using SYSTAT ver 7.0 (SPSS Inc., Chicago, IL).

Hansch Parameters. For each substituent, classical Hansch parameter values for π, σ, and E_s were obtained from a comprehensive reference (ref 21). For any one substituent, this reference cites several reported numerical values for π, σ, and E_s. The median value was used (Table 1).

Briefly, π, σ, and E_s characterize substituent hydrophobicity, electronic withdrawing ability, and molecular size, respectively. π, σ, and E_s values are relative to hydrogen, whose π, σ, and E_s values are zero. π is generally the difference of log *P* values between the substituted compound and its parent. Positive π values represent lipophilic substituents, relative to hydrogen. σ measures the substituent's ability to attract electrons. Positive σ values representing electron-withdrawing character, rather than electron-donating character. E_s is a measure of the substituent's steric bulk. Because substituents are generally larger than hydrogen and hinder reactivity, E_s values are generally negative. As discussed in the Results and Discussion section, the parameter π_- was devised. π_- only allows for Hansch π values that are negatively valued; positively valued π were set to zero for π_-. Similarly, the parameter π_+ was devised, with π_+ only allowing for Hansch π values that are positively valued; negatively valued π were set to zero for π_+.

Comparison of Computational Chemistry versus Hansch Molecular Descriptors to Explain Substituent Efect. Caco-2 permeability values were regressed via multiple linear regression against the molecular descriptor values from both the computational chemistry approach and from Hansch. Regression was performed using the MLR module of SYSTAT. In the computational chemistry approach, the following molecular descriptors were considered: ΔG_w, ΔG_h, $SASA_w$, $SASA_h$, PSA_w, PSA_h, fPSA_w, fPSA_h, CDS_w, CDS_h, and M_w. The square of each of these parameters was also considered. Forward stepwise regression was used to arrive at a model.[32,33] Regression was also pursued via the parameter reduction method.[32,33] Briefly, in the parameter reduction method, a subset of descriptors that were not collinear were identified and subjected to further analysis; the other descriptors were eliminated because each was collinear with one of the retained descriptors. The degree of collinearity between each pair of molecular descriptors was assessed via Pearson's coefficient. As described in the Appendix, all molecular descriptors except ΔG_w were collinear (i.e., Pearson's $r > 0.75$) with at least one other nonsquared descriptor, such that only four descriptors were selected for further consideration (ΔG_w, PSA_w, ΔG_h, CDS_h, along with PSA_w^2). Each squared descriptor (i.e., descriptor raised to the power 2) was collinear with its nonsquared descriptor. As described in the Results and Discussion section, the final model included ΔG_w and PSA_w^2.

In the Hansch approach, the following molecular descriptors were considered: π, π_+, π_-, σ, and E_s, as well as their squares. Both forward stepwise regression and the parameter reduction method were used to arrive at a model that related permeability to Hansch parameters.

The predictability of the final model was evaluated by cross-validation via the "leave-one-out" method. The model was rederived using the remaining 14 compounds, which was subsequently employed to predict the permeability of the excluded compound. In this regard, 14 compounds served

(31) Palm, K.; Luthman, K.; Ungell, A. L.; Strandlund, G.; Artursson, P. Correlation of drug absorption with molecular surface properties. *J. Pharm. Sci.* **1996**, *85*, 32−39.

(32) Kleinbaum, D. G.; Kupper, L. L.; Muller, K. E. *Applied Regression Analysis and Other Multivariate Methods*; PWS−Kent Publishing Company: Boston, MA, 1999.

(33) Rothman, E. D.; Ericson, W. A. *Statistics: Methods and Applications*; Kendall/Hunt Publishing Co.: Dubuque, IA, 1987.

Table 2. Caco-2 Permeability Values and Computational Property Values[a]

substituent	permeability $\times 10^6$ (cm/s)[d]	pK_a	ΔG_w (kcal/mol)	$SASA_w$ (Å^2)	PSA_w (Å^2)	fPSA_w	CDS_w (kcal/mol)	HB[e]	ΔG_h (kcal/mol)	$SASA_h$ (Å^2)	PSA_h (Å^2)	fPSA_h	CDS_h (kcal/mol)	M_w
3-COO^- [b]	6.40 (0.33)	4.82[c]	−71.97	283.1	172.5	0.61	−7.2	3	−5.64	358.6	164.0	0.46	−2.95	122.1
4-NH_2 [b]	29.1 (1.1)	9.11[c]	−71.11	248.3	130.2	0.52	−4.22	4	−6.26	329.8	125.3	0.38	−3.28	95.1
3-$CONH_2$	52.9 (1.1)	4.48	−14.09	288.6	179.0	0.62	−6.23	5	−7.18	367.1	174.6	0.48	−3.54	122.1
3-Cl	60.2 (5.5)	2.84[c]	−4.59	257.3	141.2	0.55	−1.06	1	−5.17	333.4	127.3	0.38	−3.85	113.5
3-CHO	65.9 (5.0)	0.97	−8.14	263.4	120.3	0.46	0.26	2	−5.72	343.9	100.0	0.29	−3.28	107.1
3-OH	78.0 (0.4)	6.13	−9.36	242.6	121.9	0.50	−5.24	3	−5.62	322.4	102.8	0.32	−2.79	95.6
3-CH_2OH	81.2 (1.3)	4.78	−8.91	265.3	119.5	0.45	−4.94	3	−5.43	356.8	104.4	0.29	−3.43	109.1
3-C_6H_5	85.9 (0.7)	3.34	−4.89	322.7	51.6	0.16	0.17	1	−8.63	438.6	35.5	0.08	−6.65	155.2
3-NH_2	95.4 (1.1)	7.52	−9.53	247.3	129.7	0.52	−5.15	4	−6.65	329.9	124.8	0.38	−3.29	95.1
3-CH_2 C_6H_5	101 (1)	6.36	−4.94	346.2	51.7	0.15	0.35	1	−9.47	470.0	35.6	0.08	−7.32	169.1
3-C_2H_5	106 (1)	5.35	−3.83	265.5	51.7	0.19	−0.12	1	−5.61	374.2	35.6	0.10	−4.11	107.2
3-H	107 (8)	5.25	−4.39	216.1	51.7	0.24	−0.54	1	−4.54	306.1	35.6	0.12	−2.92	79.1
3-CH_3	109 (4)	5.70[c]	−4.06	241.3	51.7	0.21	−0.3	1	−5.11	341.5	35.6	0.10	−3.54	93.1
3-F	129 (9)	1.94	−3.24	230.0	96.4	0.42	0.26	2	−3.55	317.0	99.6	0.31	−2.26	98.1
4-C_6H_5	130 (7)	5.40	−4.96	322.8	51.8	0.16	0.15	1	−8.68	438.8	35.7	0.08	−6.66	155.1

[a] Computational properties include the pK_a of the pyridine nitrogen, the free energy of solvation (ΔG, kcal/mol), the solvent accessible surface area (SASA, Å^2), the polar surface area (*PSA*, Å^2), the fraction of *PSA* (f*PSA*), the cavitation energy (CDS, kcal/mol), and the number of hydrogen bonds (HB). The environment is indicated by the subscripts w (water) or h (hexane). The polar surface area is the sum of the surface area from nitrogen, oxygen, fluorine, chlorine, and their attached hydrogens. f$PSA = PSA$/SASA [b] The 3-COOH substituent (p$K_a = 2.00$) and the pyridine nitrogen of 4-amino pyridine were treated as ionized in water and neutral in hexane. [c] Experimental pK_as from the Handbook of Chemistry and Physics, 84th edition. [d] Mean (SEM) [e] Hydrogen bond number (*HB*) included lone electron pairs (i.e., hydrogen bond acceptors) and hydrogens attached to an N or O (i.e., hydrogen bond donors).

as a training set and the to-be-predicted compound served as a test compound. This procedure was repeated until the permeability of each compound had been predicted once (i.e., until each compound served as the test compound). Model predictability was assessed through

$$Q^2 = 1 - \frac{\sum(y_{\text{pred}} - y_{\text{obs}})^2}{\sum(y_{\text{obs}} - y_{\text{mean}})^2} \qquad (2)$$

where Q^2 is the cross-validated r^2 value. Models that perfectly predict observed values result in $Q^2 = 1$, whereas models that predict as poorly as chance alone result in $Q^2 = 0$. For permeability models with two or more descriptors, partial regression analysis was used to assess the relative importance of each descriptor to modulate permeability.[32,33]

Results and Discussion

Substituent Effect on Pyridine Permeability across Caco-2 Monolayers. The permeabilities of parent pyridine and its 14 monosubstituted congeners were determined in the A−B and B−A directions. For each pyridine, A−B permeability was within 20% of the B−A permeability, indicating that each compound was effectively not transported by any active influx or efflux mechanism. Hence, only A−B permeability values were further considered and reflect passive Caco-2 permeability values.

In Table 2, substituted pyridines exhibited a wide range of permeabilities. Permeability values ranged from 6×10^{-6} cm/s to 130×10^{-6} cm/s. Parent pyridine provided a relatively high permeability of 107×10^{-6} cm/s. The ionized pyridines (i.e., 3-carboxy pyridine and 4-amino pyridine) exhibited the lowest permeability, whereas nonpolar alkyl substituents tended to yield the highest values. The rank-order substituent effect on pyridine permeability was the following: 3-COO^- < 4-NH_2 < 3-$CONH_2$ < 3-Cl < 3-CHO < 3-OH < 3-CH_2OH < 3-C_6H_5 < 3-NH_2 < 3-$CH_2C_6H_5$ < 3-C_2H_5 < **3-H** < 3-CH_3 < 3-F < 4-C_6H_5. There was a major ring position effect on amino substitution. 4-NH_2 substitution substantially reduced permeability more than 3-NH_2 substitution. Also of note, 3-C_6H_5 substitution reduced permeability relative to parent pyridine, whereas 4-C_6H_5 substitution increased permeability. This observation is consistent with the membrane transport model where minimal cross-sectional area hinders transport.[34]

The rank-order results are similar to the results of Mayer et al., who measured the intrinsic permeability of substituted *p*-toluic acids and *p*-methylhippuric acids.[17] Six substituents were common to both the present study and the work by Mayer et al.,[17] who presented data in terms of intrinsic permeability by normalizing apparent permeability for the degree of ionization. Without this normalization, the rank-order apparent permeabilities from Mayer et al. are the following: −COO− < −$CONH_2$ < −OH < −CH_2OH < −Cl < −H.[17,35] This rank order is similar to the present study of pyridine permeability across Caco-2 monolayers, which showed: 3-COO^- < 3-$CONH_2$ < 3-Cl < 3-OH < 3-CH_2-OH < 3-H. The difference between the present study and Mayer et al.[17] is 3-Cl in the present study reduced perme-

(34) Xiang, T. X.; Anderson, B. D. Influence of chain ordering on the selectivity of dipalmitoylphosphatidylcholine bilayer membranes for permeant size and shape. *Biophys. J.* **1998**, *75*, 2658−2671.

(35) Xiang, X.; Anderson, B. D. Substituent contributions to the transport of substituted *p*-toluic acids across lipid bilayer membranes. *J. Pharm. Sci.* **1994**, *83*, 1511−1518.

ability to a greater extent than 3-OH and 3-CH_2OH. Nevertheless, there is good rank-order agreement for the substituent effect between studies.

It is notable that the present pyridine studies employed Caco-2 monolayers, whereas Mayer et al.[17] used artificial lipid systems, namely, large unilamellar vesicles for *p*-methylhippuric acid studies and planar egg lectin/decane bilayers for *p*-toluic acid studies. From the six substituents common to the three data sets, substituents modulated Caco-2 permeability 17-fold. These same substituents modulated permeability over 1000-fold across artificial lipid systems.[17] These observations point toward biological bilayers (e.g., Caco-2 monolayers) as being less sensitive to substituent effects, relative to artificial membrane systems. Using substitutent *p*-methylhippuric acids, Xiang and Anderson[18] found that incorporation of a membrane protein into egg-based phosphatidylcholine bilayer compressed the range of substituent effect on permeability. Hence, it is possible here that membrane proteins within the Caco-2 apical membrane contribute to reduce the sensitivity of Caco-2 membranes to substituent effects, relative to artificial bilayers.

It should be noted that parent pyridine exhibited a relatively high Caco-2 permeability. Pyridine permeability across filters with no cells was $125(\pm 9) \times 10^{-6}$ cm/s. Hence, only 14% of the resistance for pyridine transport across Caco-2 cells was due to the Caco-2 monolayer, with the remaining 86% due to the "aqueous boundary layer" (i.e., filter plus stagnant diffusion layer).[36] Figure 2 illustrates pyridine transport across a lipid bilayer, including the potential role of the aqueous boundary layer (i.e., step 1) to limit permeability. Because of aqueous boundary layer-controlled transport of parent pyridine, there was greater allowance for substituents to decrease pyridine permeability than to increase permeability. In Table 2, substituents were able to markedly reduce permeability but only increase permeability very slightly. Hence, the chemical substituent effect on Caco-2 permeability in Table 2 reflects a substituent effect for a high-permeability parent.

Molecular Descriptor Values from the Computational Chemistry Approach. Table 2 lists molecular descriptor values from computational chemistry calculations. Free energies of solvation were negatively valued, reflecting the thermodynamic favoring of all pyridines to be solvated by both water and hexane. Compared to ΔG_h, ΔG_w showed a much wider range of values, with the ionized pyridines possessing large, negative ΔG_w values.

As expected, substitution increased solvent accessible surface area. $SASA_h$ was typically 90 Å^2 larger than $SASA_w$ because hexane is larger than water. Substitution either increased polar surface or had no effect. As expected, PSA_w was larger than PSA_h because water is a smaller probe than hexane, such that water more thoroughly probed the van der Waals surfaces of the polar atoms. PSA_w varied 3-fold across substituents, whereas PSA_h varied 5-fold. Because PSA_w values were larger than the corresponding PSA_h values, fPSA_w was larger than fPSA_h.

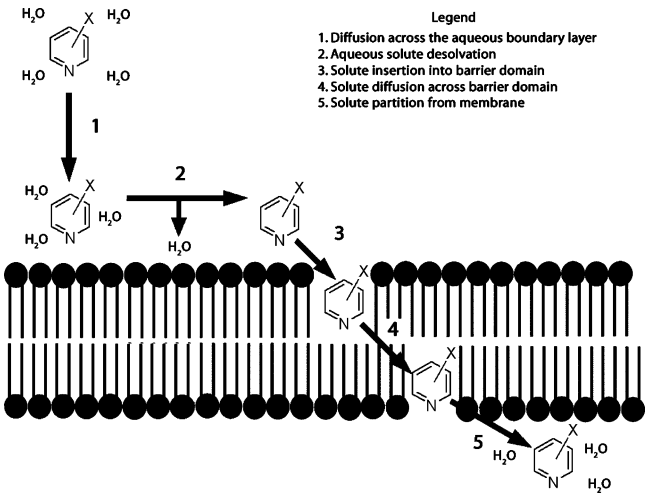

Figure 2. Solute transport across a lipid bilayer. For solutes with high bilayer permeability, diffusion across the "aqueous boundary layer" is rate-limiting. At the bilayer level, the solubility-diffusion model for membrane transport highlights (a) solute partitioning from solution into the membrane and (b) solute diffusion across the membrane barrier domain as kinetic steps in membrane permeation (refs 37−39). Partitioning is composed of aqueous solute desolvation and subsequent solute insertion into the membrane barrier domain. Legend: 1, diffusion across the aqueous boundary layer; 2, aqueous solute desolvation; 3, solute insertion into barrier domain; 4, solute diffusion across barrier domain; 5, solute partition from membrane.

As expected, the cavitation energy was dependent on solvent and pyridine substitution. All CDS_h were negatively valued (i.e., thermodynamically favorable), whereas CDS_w was either positively valued or negatively valued, depending upon substituent. Cavity formation in water without subsequent solute insertion was energetically unfavorable because of the loss of water−water hydrogen bonding, whereas cavitation in nonpolar solvents (e.g., hexane) was entropically favorable because nonpolar solvent molecules became less ordered. When pyridine was placed in an aqueous cavity, the unfavorable thermodynamics from cavitation was compensated by favorable solute−solvent dispersion interactions, such that polar substituents (e.g., 3-COO^- and 3-$CONH_2$ in Table 2) provided thermodynamically favorable values (i.e., $CDS_w < 0$). Meanwhile, nonpolar substituents (e.g., 3-CH_3 and 3-C_6H_5) resulted in CDS_w values being approximately zero or greater than zero. Unlike in water, each pyridine in hexane exhibited favorable cavitation energy, in part because solvent−solvent hydrogen bond loss was not an issue and because favorable dispersion may be introduced with pyridine insertion into the cavity. Hydrogen bond number and molecular weight are also listed in Table 2.

(36) Yu, H.; Sinko, P. J. Influence of the microporous substratum and hydrodynamics on resistances to drug transport in cell culture systems: calculation of intrinsic transport parameters. *J. Pharm. Sci.* **1997**, *86*, 1448−1457.

Table 3. Single Linear Regression Results

computational molecular descriptor	qualitative relationship with permeability[a]	r^2
ΔG_w	positive[b]	0.63
$SASA_w$	zero	<0.01
PSA_w	negative	0.57
fPSA_w	negative	0.48
CDS_w	positive	0.44
HB	negative	0.29
ΔG_h	zero	<0.01
$SASA_h$	zero	0.02
PSA_h	negative	0.52
fPSA_h	negative	0.47
CDS_h	zero	0.06
M_w	zero	<0.01

[a] Qualitative relationship indicates the sign of the coefficient. Positive and negative indicate an increasing or decreasing, statistically significant (i.e., $p > 0.05$) linear relationship between the molecular descriptor and permeability, respectively. Zero indicates a lack of a significant (i.e., $p < 0.05$) linear relationship. [b] ΔG_w values (and ΔG_h values) were negative for each pyridine.

Computational Chemistry Molecular Descriptors to Explain the Substituent Effect. Simple (or single) linear regression was performed to elucidate the influence of each computational parameter on permeability. Table 3 lists the regression results. ΔG_w was the parameter with the strongest linear relationship with permeability ($r^2 = 0.63$), whereas ΔG_h was not correlated with permeability. After ΔG_w, PSA_w and PSA_h showed the second and third strongest relations with permeability ($r^2 = 0.57$ and 0.52, respectively). Consequently, permeability correlated with each fPSA_w and fPSA_h, although not as strongly as PSA_w and PSA_h. These favorable results for *PSA* are consistent with previous findings between permeability and *PSA*.[5−8,10] Artursson and colleagues appear to suggest that the ability of *PSA* to predict permeability is underpinned by *PSA*'s hydrogen bonding character.[1] Total solvent accessible surface area (*SASA*) in water and hexane did not correlate with permeability, as previous studies found.[1,6]

As a single parameter, the number of hydrogen bonds (*HB*) provided a modest correlation ($r^2 = 0.29$), given the apparent simplicity of this parameter, where each hydrogen bond is assumed to provide the same interaction strength. Molecular weight had no effect on permeability, perhaps because molecular weight only varied over a narrow range.

The forward stepwise regression approach and the parameter reduction method each yielded the following as the best

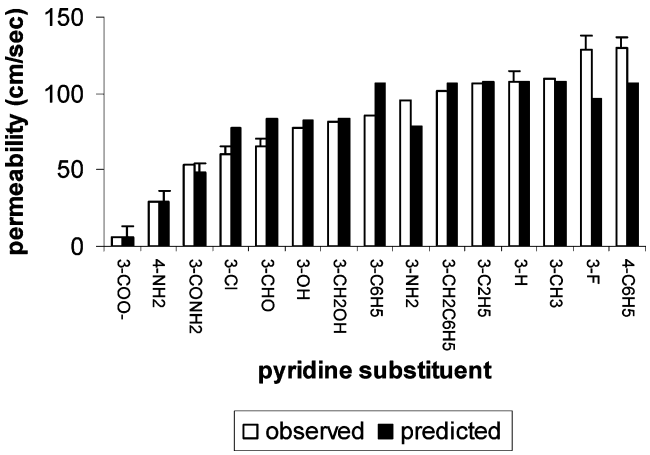

Figure 3. Observed and predicted permeability values. Predicted values were based upon eq 3 (i.e., computational approach). Error bars represent SEM and illustrated when sufficiently large to drawn clearly.

model to relate permeability to the computational molecular descriptors:

$$Papp = A\Delta G_w + B\,PSA_w^{\,2} + C \qquad (3)$$

Table 4 summarizes the model. The majority of the substituent effect on permeability can be attributed to ΔG_w and the square of PSA_w ($r^2 = 0.80$). It should be noted that raw, and not mean, permeability values were used in regression analysis. Figure 3 illustrates observed and predicted pyridine permeabilities. Cross-validation analysis showed the model to be predictive ($Q^2 = 0.77$). ΔG_w and PSA_w^2 were not strongly collinear ($r^2 = 0.29$).

Equation 3 reflects the above discussion, where parent pyridine was recognized as highly permeable, and chemical substituents reduced permeability significantly, but did not increase permeability appreciably. In eq 3, $C = 116 \times 10^{-6}$ cm/s is consistent with the observed parent pyridine permeability of $125(\pm 9) \times 10^{-6}$ cm/s across filters without a cell monolayer. The constant *C* reflects aqueous boundary layer-controlled transport, under the hydrodynamic conditions applied (50 rpm). The positive-valued coefficient for ΔG_w and the negatively valued coefficient for PSA_w^2 indicate that addition of a chemical substituent onto parent pyridine will generally reduce permeability, except for nonpolar alkyl substituents. Parent pyridine (i.e., −H substituent) possessed a slightly negative ΔG_w and a small PSA_w, such that parent pyridine was highly permeable (107×10^{-6} cm/s in Table 2). Substitution that yielded pyridines with very favorable

Table 4. Final Models from the Computational and Hansch Approaches

	computational approach	Hansch approach
model and model parameters	$Papp = A\Delta G_w + B\,PSA_w^2 + C$ where $A = 0.801(\pm 0.124) \times 10^{-6}$ cm/s per kcal/mol, $B = -0.00174(\pm 0.00029) \times 10^{-6}$ cm/s per Å^2, and $C = 116(\pm 4) \times 10^{-6}$ cm/s	$Papp = A\pi_- + C$ where $A = 23.3(\pm 3.1) \times 10^{-6}$ cm/s and $C = 97.0(\pm 4.0) \times 10^{-6}$ cm/s
fit	$r^2 = 0.80$	$r^2 = 0.58$
	$p \ll 0.001$ for all parameters	$p \ll 0.001$ for all parameters
validation	$Q^2 = 0.77$	$Q^2 = 0.34$

free energies of aqueous solvation (i.e., $\Delta G_w \ll 0$) and/or substitution that result in pyridines with large PSA_w reduced permeability significantly.

Partial regression analysis indicated that ΔG_w and PSA_w^2 were about equally influential on permeability, but varied with substituent. Permeability was reduced by approximately 1×10^{-6} cm/s for each 1 kcal/mol in ΔG_w, as well as for each 25 Å^2 of PSA_w. For example, 3-COO^- and 4-NH_2 resulted in the lowest permeabilities due to significant ΔG_w effects, as well as through PSA_w. 3-$CONH_2$ and 3-Cl resulted in low permeabilities, largely through the substituents' effects on PSA_w^2.

Of note is the position effect for the amino substituent. Because of resonance effects, 4-NH_2 resulted in the pyridine ring nitrogen to be ionized at pH 6.8, whereas 3-NH_2 did not have this effect. Although 4-NH_2 and 3-NH_2 have essentially the same PSA_w, 4-NH_2 has a much more thermodynamically favorable ΔG_w than 3-NH_2, resulting in the 4-NH_2 pyridine having a much lower permeability than 3-NH_2 pyridine. However, the computational chemistry model was not successful in predicting the positional effect for C_6H_5 because the computational model failed to capture the important molecular shape differences between 4-C_6H_5 pyridine and 3-C_6H_5 pyridine. The para substitution of 4-C_6H_5 provides a more "narrow" solute, as compared to the meta substituted 3-C_6H_5 pyridine. The present experimental results are consistent with narrow solutes being more permeable than wider solutes.[34]

Model based upon Hansch Parameters. The forward stepwise regression approach and the parameter reduction method each yielded the following as the best model to relate permeability to Hansch parameters:

$$Papp = A\pi_- + C \tag{4}$$

Table 4 summarizes the model. Substituent effect on permeability was largely attributed to π_- ($r^2 = 0.58$). Cross-validation analysis showed the model to be moderately predictive ($Q^2 = 0.32$). Molecular descriptors from the computational chemistry model (eq 3) provided a better model than one based on Hansch parameters (eq 4). Equation 4 reflects discussions above that substituents can largely only lower parent pyridine permeability. π_- is either negatively valued or zero, and is never positively valued. π_- assumes the values of π that are negative; substituents with positively valued π are assigned a π_- value of zero. Permeability was reduced by approximately 1×10^{-6} cm/s for each 0.05 π_-.

Comparison of Computational Chemistry versus the Hansch Approach to Explain the Substituent Effect. One objective of this work was to compare the relative abilities of molecular descriptors from a computational chemistry approach and molecular descriptors from the Hansch approach to explain the chemical substituent effect on pyridine permeability. The computational approach performed better than the Hansch method in three ways. First, the computational approach provided a better model fit ($r^2 = 0.80$ for eq 3 vs $r^2 = 0.58$ for eq 4) and better predictability ($Q^2 = 0.77$ vs $Q^2 = 0.34$). The basis for this better performance by computational descriptors is discussed below, along with insight provided by the computational descriptors.

Second, the computational approach performed better because the Hansch approach was practically more complex. π_- was considered only after the construction of the computational chemistry-based model and after considerable examination of the Hansch parameters π, σ, and E_s. Use of only parameters π, σ, and E_s led to a poorer model ($r^2 = 0.51$) than considering π_- alone. Meanwhile, eq 3 was achieved through common regression methods and was more straightforward to obtain, even though the computational approach considered more variables (i.e., ΔG_w, $SASA_w$, PSA_w, fPSA_w, CDS_w, HB, ΔG_h, $SASA_h$, PSA_h, fPSA_h, CDS_h, and M_w).

This difference between the computational and Hansch approaches leads to a third relative benefit of the computational chemistry-based approach: molecular descriptors from the computational approach provide more insight than Hansch parameters. The Hansch approach implicated reduced partitioning as the basis for chemical substituent effect on pyridine permeability. However, the computational approach more specifically identified aqueous desolvation, and not overall partitioning. This advantage of greater specificity of the computational approach is discussed immediately below.

Insight from Computational Molecular Descriptors. The solubility-diffusion model outlines the physicochemical basis for solute permeability across a lipid membrane.[37−39] This model highlights (a) solute partitioning from solution into the membrane and (b) solute diffusion across the membrane as kinetic steps in membrane permeation. The solubility-diffusion model is generally expressed as

$$P_m = \frac{K_m D_m}{d_m} \tag{5}$$

where P_m is the solute permeability across the membrane, K_m is the partition coefficient of the solute between the solvent and membrane, D_m is the diffusion coefficient of the solute in the membrane, and d_m is the membrane thickness. As written, eq 5 implicates membrane homogeneity of K_m, D_m, and d_m to reflect average membrane properties. Lipid bilayers, such as cell plasma membranes, are heterogeneous.[40,41] Anderson and colleagues[42,43] have elucidated that

(37) Diamond, J. M.; Wright, E. M. Biological membranes: the physical basis of ion and nonelectrolyte selectivity. *Annu. Rev. Physiol.* **1969**, *31*, 581−646.

(38) Walter, A.; Gutknecht, J. Permeability of small nonelectrolytes through lipid bilayer membranes. *J. Membr. Biol.* **1986**, *90*, 207−2017.

(39) Finkelstein, A. *Water Movement through Lipid Bilayers, Pores, and Plasma Membranes: Theory and* Reality; Wiley-Interscience: New York, 1987.

(40) Tieleman, D. P.; Marrink, S. J.; Berendsen, H. J. A computer perspective of membranes: molecular dynamics studies of lipid bilayer systems. *Biochim. Biophys. Acta* **1997**, *1331*, 235−270.

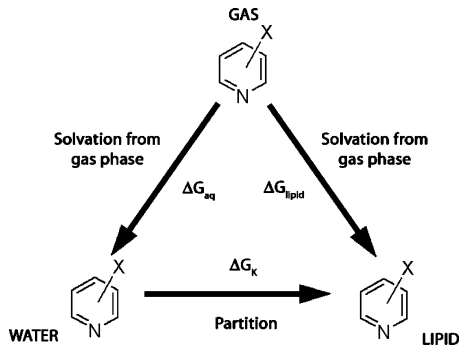

Figure 4. Thermodynamic cycle for the partitioning of a pyridine between an aqueous phase and a lipid phase. ΔG_{aq} and ΔG_{lipid} are the free energies of solvation from the gas phase into water and lipid, respectively. ΔG_K is the free energy of partitioning from the aqueous phase into lipid and is equal to $\Delta G_{lipid} - \Delta G_{aq}$. In the context of Figure 2, solute transport will require solute partioning via (a) aqueous solute desolvation (step 2 in Figure 2) and (b) subsequent solute insertion into barrier domain (step 3 in Figure 2). Figure 4 indicates the two component processes of partitioning are determined by ΔG_{aq} and ΔG_{lipid}, respectively.

the ordered hydrocarbon chain region of a bilayer is the barrier domain for polar solutes, such that

$$P_m = \frac{K_{bd/w} D_{bd}}{d_{bd}} \qquad (6)$$

where $K_{bd/w}$ is the barrier domain/water partition coefficient, D_{bd} is the diffusion coefficient of the solute in the barrier domain, and d_{bd} is the barrier domain thickness.

The partition coefficient can be estimated from the thermodynamics of solute solvation into each phase. Figure 4 illustrates the thermodynamic cycle for the partitioning of a pyridine between an aqueous phase and a lipid phase. The partition coefficient is

$$\log K = \frac{-1}{2.303RT}(\Delta G_{lipid} - \Delta G_{aq}) \qquad (7)$$

where K is the partition coefficient between the lipid and aqueous phases, ΔG_{aq} is the free energies of solvation from the gas phase into water, and ΔG_{lipid} is the free energy of solvation from the gas phase into lipid. Using eq 7, log K was calculated from ΔG_w and ΔG_h. Table 5 shows the strength of linear associate between several variables. Log K is, of course, perfectly correlated with $\Delta G_h - \Delta G_w$.

Table 5. Correlation Coefficient for the Linear Relationship between Selected Parameters[a]

relationship	linear r^2
log K vs $\Delta G_w + \Delta G_h$	1.0
log K vs ΔG_w	0.99 ($r^2 = 0.75$ if 3-COO^- and 4-NH_2 excluded)
log K vs ΔG_h	0.01
ΔG_w vs ΔG_h	<0.01
permeability vs π	0.51
permeability vs π_-	0.58
permeability vs π_- (exclude 4-NH_2)	0.62
permeability vs log K	0.63
permeability vs ΔG_w	0.63
ΔG_w vs π	0.50
[log K vs π]	[0.53]
ΔG_w vs π (exclude all data with $\pi > 0$ as well as 4-NH_2 data)	0.95
[log K vs π (exclude all data with $\pi > 0$ as well as 4-NH_2 data)]	[0.93]

[a] The results indicate that aqueous desolvation to underpin the substituent effect on permeability, including the basis for permeability's apparent dependence on Hansch lipophilicy.

However, the substituent effect on log K is completely explained by ΔG_w ($r^2 = 0.99$), with ΔG_h having no impact on log K ($r^2 < 0.01$).

These relationships indicate that pyridine permeability was not controlled by partitioning per se, but controlled by aqueous desolvation. In Table 5, π was able to explain only 51% of the substituent effect on permeability. Substituents with positively valued π did not appreciably increase permeability because of parent pyridine's high permeability. In Table 5, π_- provided $r^2 = 0.58$ with permeability. π_- produced $r^2 = 0.62$ with permeability when 4-NH_2 was dropped; the Hansch parameter π cannot account for 4-NH_2's modulation of the ring nitrogen protonation state. The correlation between ΔG_w and permeability ($r^2 = 0.63$ without 4- NH_2) essentially matched the correction between π_- and permeability because ΔG_w explains π_-. Figure 5 illustrates the relation between π and ΔG_w. For the majority of substituents, π can be explained by ΔG_w, particularly for $\pi \leq 0$ ($r^2 = 0.95$). These results mimic the essentially complete dependence of log K on ΔG_w. Given this relationship and the observation that π_- constituted the best Hansch model to explain pyridine permeability (eq 4), it appears that aqueous desolvation, and not partitioning per se, is the kinetic barrier for permeation by pyridines. Partitioning can be considered to be composed of solute aqueous desolvation, with subsequent insertion of the solute into the membrane (Figures 2 and 4). Only aqueous desolvation was able to limit pyridine permeability. Pyridine insertion into the membrane did not limit pyridine permeability, as evidenced by the lack of correlation between pyridine permeability with either ΔG_h or CDS_h (Table 3).

Permeability analysis that considers the aqueous boundary layer[36] suggests that the nine least-permeable pyridines (i.e.,

(41) Polli, J. E.; Balakrishnan, A.; Seo, P. R. Human Intestinal Cellular Characteristics and Drug Permeability. In *Cellular Drug Delivery: Present and Potential*; Lu, Oie, R.; S., Eds.; Humana Press: Totowa, NJ, 2004; pp 163−180.

(42) Xiang, T. X.; Anderson, B. D. A computer simulation of functional group contributions to free energy in water and a DPPC lipid bilayer. *Biophys J.* **2002**, *82*, 2052−2066.

(43) Mayer, P. T.; Xiang, T. X.; Niemi, R.; Anderson, B. D. A hydrophobicity scale for the lipid bilayer barrier domain from peptide permeabilities: nonadditivities in residue contributions. *Biochemistry* **2003**, *42*, 1624−1636.

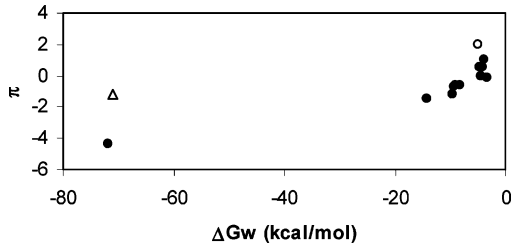

Figure 5. Relation between π and ΔG_w. For a majority of substituents, π can be explained by ΔG_w, particularly for hydrophilic substituents (i.e., $\pi < 0$). The large π of 3-$CH_2C_6H_5$, 3-C_6H_5, and 4-C_6H_5 (open circles) is not reflected by ΔG_w because the hydrophobicity of the substituents is benefited from their favorable ΔG_h. In contrast to 3-NH_2, 4-NH_2 (open triangle) did not follow the general pattern between π and ΔG_w because of the inability of π_- to anticipate resonance effects on the pyridine ring nitrogen.

3-COO^-, 4-NH_2, 3-$CONH_2$, 3-Cl, 3-CHO, 3-OH, 3-CH_2OH, 3-C_6H_5, and 3-NH_2) exhibited transport that was globally controlled by the Caco-2 monolayer. The remaining pyridines were aqueous boundary-layer-controlled. Control of pyridine permeability by these nine substituents is based upon the ability of each of these substituents to hinder pyridine desolvation from water, and generally occurred when $\Delta G_w < -8$ kcal/mol. In Table 5, correlation analysis between ΔG_w and π reiterates this finding. The linear r^2 for ΔG_w versus π was 0.95 for hydrophilic substituents (i.e., $\pi < 0$), excluding 4-NH_2.

The above analysis indicated that molecular descriptors from the computational chemistry approach were more insightful than Hansch descriptors. The computational approach included solvent−solute interactions (i.e., solvent-pyridine interactions). For example, the free energies of solvation and cavitation energies were computed. The vast majority of computational methods that describe permeability in terms of molecular descriptors only consider the solute, and not explicit solvent−solute interactions, even though aqueous desolvation has been implicated in determining solute permeability.[22] Computational descriptors highlight ΔG_w and PSA_w^2 (eq 3) as surrogates for transport resistance across Caco-2 monolayers. Because ΔG_w directly measures aqueous solvation theromodynamics, ΔG_w is interpreted to reflect the aqueous desolvation barrier. Artursson and collegues appear to suggest that the ability of *PSA* to predict permeability is underpinned by *PSA*'s hydrogen bonding character.[1] Hence, PSA_w is also interpreted here to reflect the aqueous desolvation barrier. These results suggest that pyridine permeability is controlled by desolvation of the pyridine from water, rather than global pyridine partitioning. Specifically, the substituent effect on permeability was mediated through the substituents' modulating effect on pyridine aqueous desolvation.

It should be noted that these substituent results would not be expected to apply to parent compounds that, unlike pyridine, are lowly permeable. For example, a parent structure with low permeability due to an already high aqueous solvation energy and high polar surface area would not be expected to be sensitive to the substituent pattern observed here for pyridine. Rather, lead structures that are lipophilic and high membrane permeability, which occurs frequently in drug design, would be more likely to follow the substituent pattern observed here.

In summary, the objective was (1) to evaluate the chemical substituent effect on Caco-2 permeability, using a congeneric series of pyridines, and (2) compare the relative abilities of molecular descriptors from a computational chemistry approach and molecular descriptors from the Hansch method, to explain the chemical substituent effect on pyridine permeability. The passive permeability of 15 members of a congeneric pyridine series were measured across Caco-2 monolayers. Results indicate a 20-fold effect of chemical substitution on Caco-2 permeability, where substituents more frequently reduced permeability than increased permeability, in part reflecting high parent pyridine permeability. The pyridines were also subjected to computational chemistry analysis to characterize each pyridine in terms of several molecular descriptions, including solvation free energies in water and polar surface area in water. Permeability was regressed against the molecular descriptors from computational chemistry, as well as classic Hansch parameters. The observed substituent effect was better explained via the molecule descriptors from the computational chemistry than classic descriptors from Hansch. Computational descriptors suggest that aqueous desolvation, but not membrane partitioning per se, was the mechanism by which chemical substituents modulated pyridine permeability.

Acknowledgment. This work was supported financially by a grant from Proctor & Gamble International Program for Animal Alternatives, a grant from NIH-NIDDK (DK 067530), and the University of Maryland School of Pharmacy Computer-Aided Drug Design Center.

Appendix. Intermediate Results from Multiple Linear Regression Analysis

This appendix provides intermediate results in conducting multiple linear regression of permeability against computational molecular descriptors via the parameter reduction

Table 6. Results from Simple Regression Analysis of Permeability as a Function of Individual Computational Parameters

parameter	r^2	coefficient × 10^6 [a]	*p* value
ΔG_w	0.63	1.20 (±0.14) (cm/s per kcal/mol)	<0.001
PSA_w	0.57	−0.573 (±0.077) (cm/s per Å)	<0.001
PSA_w^2	0.60	−0.00276 (±0.00034) (cm/s per Å^2)	<0.001
ΔG_h	<0.01	0.27 (±3.36) (cm/s per kcal/mol)	<0.01
CDS_h	0.06	−5.71 (±3.46) (cm/s per kcal/mol)	0.10

[a] Mean (±SEM).

method. The parameter reduction method was carried out in addition to forward stepwise regression because forward stepwise regression does not guarantee arrival at the best model.

In the parameter reduction method, a subset of descriptors that are not collinear are identified and subjected to further analysis; the other descriptors are eliminated because each is collinear with one of the retained descriptors. The degree of collinearity between each pair of molecular descriptors was assessed via Pearson's coefficient from SYSTAT. All molecular descriptors except ΔG_w were collinear (i.e., Pearson's $r > 0.75$) with at least one other nonsquared descriptor (data not shown). Each squared descriptor (i.e., descriptor raised to the power 2) was collinear with its nonsquared descriptor. ΔG_w, PSA_w, ΔG_w, and CDS_h were selected for further consideration, by virtue of their simplicity (compared to squared terms) and their collective collinearity with all other parameters. PSA_w and PSA_h were essentially perfectly collinear, with Pearson $r = 0.99$. Although either could have been selected, PSA_w was selected over PSA_h because PSA_w is frequently used to explain permeability.

Table 6 shows the single regression analysis results of permeability versus each ΔG_w, PSA_w, ΔG_h, CDS_h, and PSA_w^2. As described in the Results and Discussion section, the final model included ΔG_w and PSA_w^2.

MP050096+